Rare Met. (2019) 38(1):81–86
https://doi.org/10.1007/s12598-018-1184-x

RARE METALS
www.editorialmanager.com/rmet

Enhancing low-temperature NO_x storage and reduction performance of a Pt-based lean NO_x trap catalyst

Tong Wang, Li-Wei Jia, Xiu-Ting Wang, Gang Wang, Fu-Qiang Luo, Jia-Ming Wang*

Received: 1 July 2018 / Revised: 29 October 2018 / Accepted: 8 November 2018 / Published online: 12 December 2018

Abstract Two lean NO_x trap (LNT) catalysts, Pt/BaO/CeO_2 + Al_2O_3 and Pt/BaO/CeO_2 − Al_2O_3, were prepared and compared for low-temperature (< 250 °C) NO_x storage and reduction performance. The influence of the form of ceria on low-temperature NO_x storage and reduction performance of LNT catalysts was investigated with the focus on NO_x storage capacity, NO_x reduction efficiency during lean/rich cycling, product selectivity and thermal stability. Inductively coupled plasma-atomic emission spectrometry (ICP-AES), Brunner–Emmet–Teller (BET), H_2-pulse chemisorption and X-ray diffraction (XRD) were conducted to characterize the physical properties of LNT catalysts. NO_x storage capacity and NO_x conversion efficiency were measured to evaluate NO_x storage and reduction performance of LNT catalysts. Pt/BaO/CeO_2 − Al_2O_3 catalyst exhibits higher NO_x storage capacity than Pt/BaO/CeO_2 + Al_2O_3 catalyst in the temperature range of 150–250 °C. Meanwhile, Pt/BaO/CeO_2 − Al_2O_3 catalyst shows better NO_x conversion efficiency and N_2 selectivity. XRD results indicate that the thermal stability of CeO_2 − Al_2O_3 complex oxide is superior to that of pure CeO_2. H_2-pulse chemisorption results show that Pt/BaO/CeO_2 − Al_2O_3 catalyst has higher Pt dispersion than Pt/BaO/CeO_2 + Al_2O_3 catalyst over fresh and aged samples. The improved physical properties of Pt/BaO/CeO_2 − Al_2O_3 catalyst are attributed to enhance the NO_x storage and reduction performance over Pt/BaO/CeO_2 + Al_2O_3 catalyst.

Keywords NO_x storage and reduction; Low temperature; Ceria; Ceria-alumina; LNT

1 Introduction

To meet the stringent China Stage-VI light-duty diesel vehicles' NO_x emission regulations, a promising approach has been explored by a combination of lean NO_x trap (LNT) and selective catalytic reduction (SCR) catalysts [1–3], which can enhance NO_x reduction while avoiding the need for urea injection to the SCR catalyst [4]. However, additional improvements are required in LNT system, especially for low-temperature NO_x conversion [5, 6].

LNT catalysts operate under cyclic lean/rich conditions [7, 8]. During lean conditions, NO_x is stored on the catalyst; while during rich conditions, stored NO_x is released and reduced into N_2 along with possible byproducts, such as NH_3 and N_2O [9–11]. A typical LNT catalyst contains basic components (alkali metal or alkaline earth metal compounds) for NO_x storage, noble metals (Pt, Pd, Rh), and support oxides [7]. In addition, ceria-based materials have been shown to be beneficial for LNT catalysts at low temperatures [12–14]. CeO_2 is a common rare earth metal oxide with special structure and properties [15–17], and many current commercial LNT catalysts have already incorporated ceria [5, 18].

In the present work, the goal was to study the effects of the form of ceria on low-temperature NO_x storage and reduction performance through surface/bulk analysis and activity tests. The first catalyst of Pt/BaO/CeO_2 + Al_2O_3

T. Wang, F.-Q. Luo
School of Automotive and Traffic Engineering, Jiangsu University, Zhenjiang 212013, China

L.-W. Jia, X.-T. Wang, G. Wang, J.-M. Wang*
Wuxi Weifu Environmental Catalysts Co. Ltd, Wuxi 214028, China
e-mail: wxt5409@126.com

used ceria as a support material as well as alumina, and the second catalyst of Pt/BaO/CeO_2 − Al_2O_3 used complex ceria–alumina as a new support material. The low-temperature NO_x storage capacity (NSC), NO_x reduction efficiency, NH_3 production and N_2O emissions were measured. Thermal stability of LNT catalysts was also investigated after aging for 20 h at 800 °C.

2 Experimental

2.1 Catalyst preparation

Catalysts were prepared by incipient wetness impregnation technique, using aqueous solutions of $Ba(CH_3COO)_2$ and $Pt(NO_3)_2$. In the preparation of Pt/BaO/CeO_2 + Al_2O_3 (1 wt% Pt and 9 wt% BaO), CeO_2 (specific surface area 152 $m^2 \cdot g^{-1}$) and γ-Al_2O_3 (150 $m^2 \cdot g^{-1}$) were mechanically mixed at the weight ratio of 3:7. The impregnation was carried out in a sequential manner: The well-mixed CeO_2 + Al_2O_3 support was firstly impregnated with the Ba acetate solution followed by Pt nitrate solution. On the other hand, Pt/BaO/CeO_2 − Al_2O_3 (1 wt% Pt and 9 wt% BaO) was prepared similarly, but using a CeO_2 − Al_2O_3 complex oxide (30 wt% CeO_2 and 70 wt% Al_2O_3, 154 $m^2 \cdot g^{-1}$) as the support. After each impregnation step, the catalyst was dried at 100 °C in air for overnight and then calcined in air at 500 °C for 5 h. The obtained fresh catalysts were denoted as F-1 and F-2, respectively. In order to compare their thermal stability, the catalysts were further calcined in air at 800 °C for 20 h. The aged catalysts were denoted as A-1 and A-2.

2.2 Catalyst characterization

The actual elemental compositions of catalysts were analyzed by inductively coupled plasma-atomic emission spectrometry (ICP-AES, Optima 2100 DV, PerkinElmer). The Brunner–Emmet–Teller (BET) specific surface areas were measured by N_2 adsorption–desorption at − 196 °C on a Micromeritics ASAP 2000 analyzer. Prior to measurements, the samples were pre-treated at 150 °C under vacuum for 3 h to eliminate the adsorbed species. The Pt dispersions were determined by H_2-pulse chemisorption at − 80 °C by a Micromeritics AutoChem II Analyzer. The crystalline phases of the catalysts were characterized by X-ray diffractometer (XRD, XRD-600, Shimadzu) with a Cu Kα radiation (λ = 0.154056 nm) at 36 kV with a graphite monochromator.

2.3 Activity measurements

In NO_x storage capacity (NSC) and NO_x conversion efficiency measurements, 0.25 g Pt/BaO/Al_2O_3 catalyst was mixed with 0.75 g quartz sand. The total flow rate is 1 $L \cdot min^{-1}$, corresponding to a space velocity of 60,000 h^{-1}. Before each experiment, the sample was oxidized in 10% O_2/N_2 balance at 350 °C for 30 min, and then reduced in 5% H_2/N_2 balance at 450 °C for 20 min. The reactor was then cooled in N_2 to the target test temperatures at 150, 200 and 250 °C. The outlet gas of the reactor was maintained at 140 °C to avoid condensation and NH_3 hold-up. A MKS MultiGas 2030 FT-IR analyzer was used to monitor NO, NO_2, N_2O, NH_3, CO, C_3H_6, CO_2 and H_2O concentrations of the outlet gas.

NO_x storage capacity (NSC) tests were conducted by exposing the catalyst to the flowing gas containing 250 × 10^{-6} NO, 8% O_2, 5% H_2O, 5% CO_2 at 150, 200 and 250 °C. The storage time was 10 min at each temperature during NSC measurement. NO_x conversion efficiency tests were also measured at 150, 200 and 250 °C, and LNT performance was evaluated in a lean/rich (100 s/17 s) cycle under the gas composition detailed in Table 1. The average value of the last 5 cycles was calculated after 15 lean/rich cycles.

3 Results and discussion

3.1 Catalyst characterization

The contents of Pt, Ba, Ce and Al in catalysts are summarized in Table 2. F-1 and F-2 samples have similar Pt and Ba contents. Ce content in F-1 is slightly lower than that in F-2 (26.24 wt% vs. 27.54 wt%).

BET specific surface areas and Pt dispersions of catalysts are listed in Table 3. The specific surface areas of F-1 and F-2 samples are 117 and 122 $m^2 \cdot g^{-1}$, respectively. Pt dispersion of F-1 is 60%, slightly lower than 62% of F-2. After thermal aging at 800 °C for 20 h, their surface areas decrease to 99 and 103 $m^2 \cdot g^{-1}$, respectively. The Pt dispersions reach significantly low values, only 12% for A-1 and 19% for A-2, indicating that the sintering of Pt particles occurs during aging due to the mobility of Pt crystallites and eventually merged to form larger particles [19].

Figure 1 shows XRD patterns of fresh and aged catalysts. The results show that Pt-related phases in all four samples were not detected because of either the low loading ratio or its small size. The main crystallite phases detected are CeO_2, $BaCO_3$ and γ-Al_2O_3 in all samples. The $BaAl_2O_4$ peak only appears after aging [20, 21]. Applying Scherrer equation, the average CeO_2 crystal size was calculated based on CeO_2 diffraction peak at 2θ = 28.5°. The

Table 1 NO_x conversion efficiency measurement: gas composition

Gas composition	NO	CO	C_3H_6	CO_2 /%	H_2O/%	O_2/%	H_2/%	N_2
Lean	250×10^{-6}	1800×10^{-6}	370×10^{-6}	5	5	10.00	–	Bal.
Rich	250×10^{-6}	3.00%	960×10^{-6}	5	5	0.60	0.25	Bal.

Table 2 Elemental composition of fresh catalysts (wt%)

Catalyst	Pt	Ba	Ce	Al
F-1	1.05	8.06	21.36	32.29
F-2	1.07	7.98	22.42	31.72

F-1—fresh $Pt/BaO/CeO_2 + Al_2O_3$ catalyst; F-2—fresh $Pt/BaO/CeO_2 - Al_2O_3$ catalyst

Table 3 BET specific surface areas and Pt dispersions of catalysts

Catalyst	Surface area/($m^2 \cdot g^{-1}$)	Pt dispersion/%
F-1	117	60
F-2	122	62
A-1	95	12
A-2	103	19

CeO_2 crystal size in F-1 is estimated to be 10 nm, while 6 nm in F-2, 16 nm in A-1, and 7 nm in A-2, respectively. These XRD results suggest that the thermal stability of $CeO_2 - Al_2O_3$ complex oxide is superior to that of pure $CeO_2 + Al_2O_3$ with regard to CeO_2 crystal size.

3.2 NO_x storage capacity (NSC)

The results of NO_x storage capacity tests are reported in Table 4. All samples' NSCs increase substantially as the test temperature increases from 150 to 250 °C due to enhancing NO oxidation activity to produce NO_2 which is known to be more effective than NO to be adsorbed on LNT catalysts [22]. F-2 sample displays higher NSC compared to F-1 sample at 150, 200 and 250 °C. NSCs of aged samples are lower than those of the fresh samples. A-2 sample still has higher NSC than A-1 sample. The NSC results indicate that $CeO_2 - Al_2O_3$ complex oxide as the support loaded with Ba and Pt can trap NO_x amount to more extent in comparison with $CeO_2 + Al_2O_3$.

Table 4 NO_x storage capacity (250×10^{-6} NO, 8% O_2, 5% H_2O, 5% CO_2, N_2 bal., GHSV = 60,000 h^{-1}) of catalysts ($\mu mol \cdot g^{-1}$)

Temperature/°C	F-1	F-2	A-2	A-2
150	36.4	39.6	32.3	36.1
200	88.2	98.5	75.4	88.0
250	226.7	243.3	164.4	188.2

3.3 NO_x conversion efficiency

NO_x concentration profiles during the last 5 lean/rich cycles are shown in Fig. 2. Average NO_x conversions during the last 5 cycles are presented in Table 5. For F-1 sample, NO_x breakthrough is immediately observed after the feed gas switched into lean condition at 150 °C, and the outlet NO_x concentration decreases with time and gradually approaches the inlet NO_x concentration. When the feed gas is subsequently switched to the rich condition, a sharp and intense NO_x release peak appears and then intensity

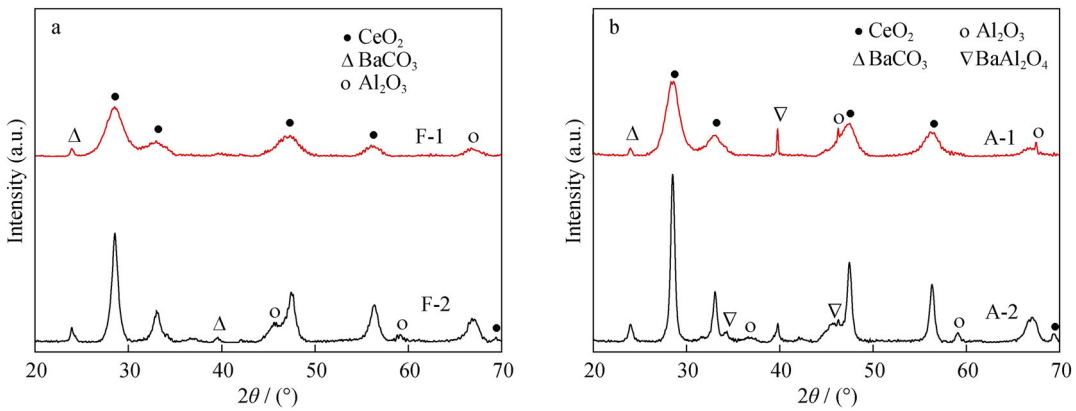

Fig. 1 XRD patterns of fresh and aged catalysts: **a** F-1 and F-2 catalysts and **b** A-1 and A-2 catalysts

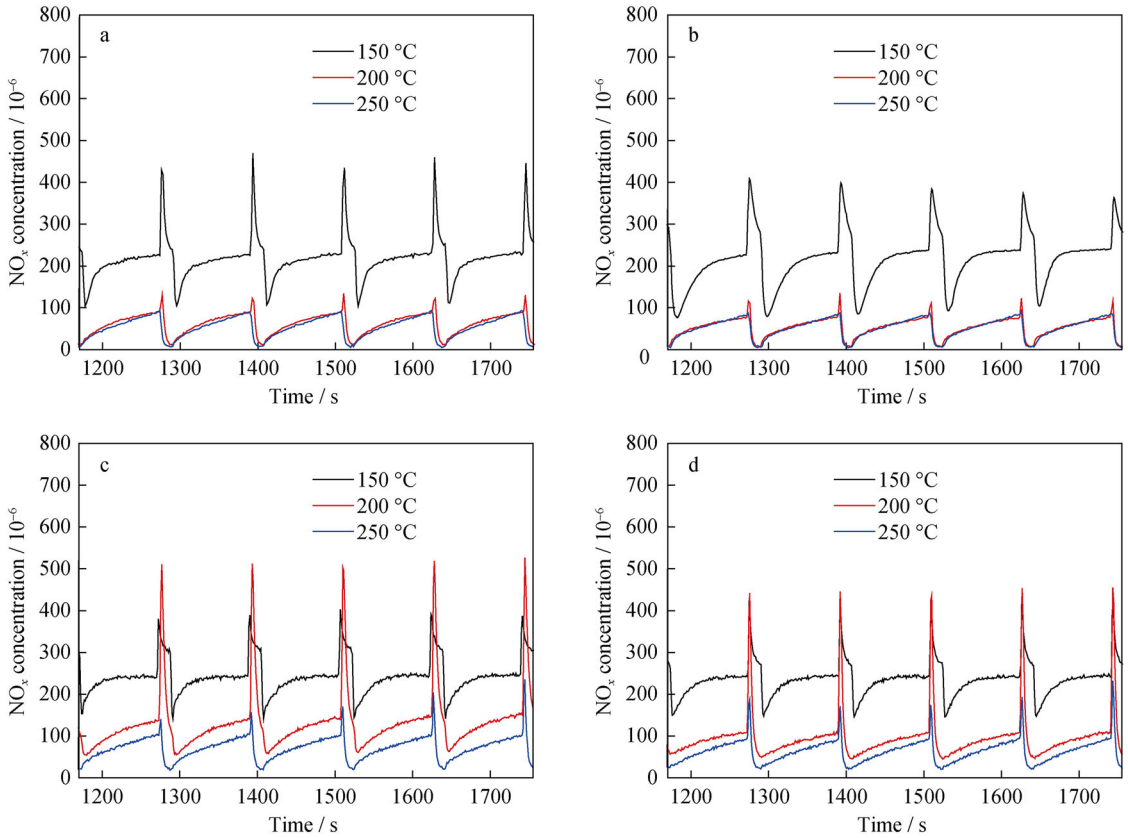

Fig. 2 NO_x concentration profiles during last 5 lean/rich cycles: **a** F-1 catalyst, **b** F-2 catalyst, **c** A-1 catalyst, and **d** A-2 catalyst

Table 5 NO_x conversion and selectivity of N-containing products during last 5 lean/rich cycles

Temperature/°C	Catalyst	NO_x conversion/%	Selectivity/%		
			NH_3	N_2O	N_2
150	F-1	13.8	8.6	51.1	40.3
	F-2	14.6	7.4	51.5	41.1
	A-1	6.6	0	66.9	33.1
	A-2	9.0	4.9	55.6	39.5
200	F-1	72.0	38.5	34.7	26.8
	F-2	73.4	29.6	33.8	36.6
	A-1	49.0	46.4	38.3	15.3
	A-2	58.9	36.4	38.2	25.4
250	F-1	75.2	22.6	23.8	53.6
	F-2	76.1	18.9	20.7	60.4
	A-1	68.4	42.3	28.6	29.1
	A-2	71.7	31.4	25.5	43.1

quickly decreases. The similar profile was also observed in a previous study [23]. The average NO_x conversion at 150 °C is 13.8%. At 200 °C, the outlet NO_x concentration reaches only about 90×10^{-6} at the end of the lean duration. The amount of NO_x release during switching to rich condition becomes significantly lower compared to that at 150 °C. Therefore, the average NO_x conversion increases to 72.0%. At 250 °C, NO_x concentration profile during lean duration is almost coincided with that at 200 °C. However, there is no NO_x release detected during switching to rich condition. Average NO_x conversion reaches 75.2%. Raising reaction temperature increases NO_x storage capacity, and on the other hand, high temperature is beneficial to promoting NO_x reduction ability. As a result, the average NO_x conversion increases with reaction temperature increasing from 150 to 250 °C.

In the case of F-2 sample, NO_x evolutions at three temperatures are similar to those of F-1 sample, but F-2 sample has slightly higher average NO_x conversions, 14.6% at 150 °C, 73.4% at 200 °C, and 76.1% at 250 °C, in accordance with the results of NSC measurements.

After thermal aging, the amount of NO_x trapped on the aged catalyst at lean phase at 150 °C becomes smaller in comparison with fresh catalysts and the outlet NO_x concentrations gradually reach a constant level (around 240×10^{-6}) for both aged catalysts. Higher NO_x slip is observed during rich phase, and average NO_x conversions of A-1 and A-2 samples are only 6.6% and 9.0%, respectively. At 200 °C, NO_x-spill-out over A-1 is relatively larger in comparison with that over A-2 during switching to

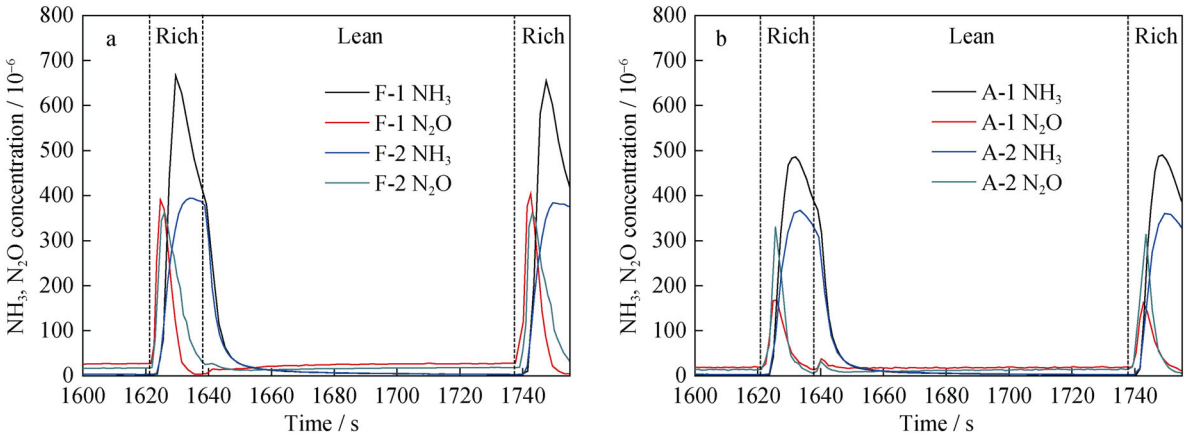

Fig. 3 Evolution of NH_3 and N_2O concentrations during lean/rich cycles at 200 °C: **a** fresh samples and **b** aged samples

the rich condition, leading to a lower NO_x conversion for A-1 (49.0% vs. 58.9% for A-2). NO_x release still appears over aged samples at 250 °C, resulting in that NO_x conversion decreases to some extent. Average NO_x conversion sharply declines at 150 and 200 °C. Pt is known to have impacts on NO oxidation under lean conditions, NO_x storage under rich/lean conditions and NO_x reduction under rich conditions [7]. The difference in NO_x conversion may be correlated with different Pt dispersions of catalysts. Clayton et al. [24] also found that the differences in storage and reduction activity were the largest among three catalysts which have different Pt dispersions at low temperatures (< 200 °C).

From the perspective of study on the law and production of NH_3 and N_2O, their concentrations evolution at 200 °C during lean/rich cycles is taken as an example and shown in Fig. 3. For fresh and aged samples, NH_3 and N_2O are both formed in lean and rich phases. During lean phase, NH_3 and N_2O are subsequently formed, NH_3 intensity sharply decreases to below 10×10^{-6} at the initial lean phase, while a small N_2O peak appears, and then the N_2O intensity gradually becomes stabilized. A sharp N_2O peak is immediately observed at the beginning of rich phase, and NH_3 peak delays about 2 s. In comparison with the results obtained over fresh samples, the amount of NH_3 and N_2O formation decreases over aged samples. In the lean and rich phase, NH_3 is mainly formed via the reduction in NO_x by surface hydrogen, although NH_3 is also a product of isocyanate hydrolysis reaction [25, 26], Dasari et al. [25] summarized the following reaction mechanism:

$$Pt - H + Pt - NO \rightarrow Pt - HNO + Pt* \quad (1)$$

$$Pt - HNO + Pt* \rightarrow Pt - NH + Pt - O \quad (2)$$

$$Pt - HNO + Pt* \rightarrow Pt - N + Pt - OH \quad (3)$$

$$Pt - NH + Pt - H \rightarrow Pt - NH_2 + Pt* \quad (4)$$

$$Pt - NH_2 + Pt - H \rightarrow Pt - NH_3 + Pt* \quad (5)$$

$$Pt - NH_3 \rightarrow NH_3 + Pt* \quad (6)$$

N_2O formation in lean phase is related to the reactions between surface-deposited reductants/intermediates (CO, HC, NH_3, isocyanate) and gaseous NO/O_2, and N_2O release peak during rich phase may be attributed to that NO_x partially reduced over platinum group metal (PGM) sites [26–28].

Concerning the product selectivity, N_2O is the main product at 150 °C. At 200 °C, selectivity of NH_3, N_2O and N_2 is similar for fresh samples, but NH_3 and N_2O become the main products for aged samples. By increasing the temperature to 250 °C, N_2 selectivity of all samples shows a substantial enhancement. Moreover, N_2O selectivity decreases as the temperature increases from 150 to 250 °C. N_2 selectivity decreases in the following order: F-2 > F-1 > A-2 > A-1. Thermal aging results are in an increase in NH_3 and N_2O selectivity, except NH_3 selectivity at 150 °C. Compared to fresh samples, the higher NH_3 selectivity over aged LNT catalysts above 200 °C was also found by Chatterjee et al. [29] and Easterling et al. [30]. Chatterjee et al. [29] suggested that the lower noble metal and oxygen storage activities correspond to the shifted light-off of the ammonia oxidation reactions to higher temperatures, which supports the faster NH_3 breakthrough.

4 Conclusion

The influence of the form of ceria on low-temperature NO_x storage and reduction performance of LNT catalysts was investigated, using $CeO_2 - Al_2O_{33}$ complex oxide or $CeO_2 + Al_2O_3$ mixed oxide as the support for BaO and Pt. $CeO_2 - Al_2O_3$ support exhibits the improvements on NO_x storage capacity, NO_x conversion efficiency (especially for aged samples at 200 °C) and N_2 selectivity in comparison

with $CeO_2 + Al_2O_3$ support in the temperature range of 150–250 °C. After aging for 20 h at 800 °C, Pt/BaO/$CeO_2 - Al_2O_3$ catalyst exhibits better thermal stability and chemical distribution than Pt/BaO/$CeO_2 + Al_2O_3$ catalyst. Overall, $CeO_2 - Al_2O_3$-based catalysts show superior NO_x storage and regeneration performance over $CeO_2 + Al_2O_3$-based catalyst at low temperatures.

Concerning NH_3 and N_2O selectivity of NO_x reduction, N_2O is the main product at 150 °C, and its selectivity decreases as the temperature increases from 150 to 250 °C. Thermal aging results are in an increase in the NH_3 and N_2O selectivity at 200 and 250 °C.

Acknowledgements This study was financially supported by the National Key R&D Program of China (No. 2017YFC0211100).

References

[1] Wang J, Ji YY, He ZW, Crocker M, Dearth M, McCabe RW. A non-NH_3 pathway for NO_x conversion in coupled LNT-SCR systems. Appl Catal B Environ. 2012;111–112:562.
[2] Liu Y, Harold MP, Luss D. Coupled NO_x storage and reduction and selective catalytic reduction using dual-layer monolithic catalysts. Appl Catal B Environ. 2012;121–122:239.
[3] Wang J, Ji YY, Jacobs G, Jones S, Kim DJ, Crocker M. Effect of aging on NO_x reduction in coupled LNT–SCR systems. Appl Catal B Environ. 2014;148–149:51.
[4] Johnson T, Joshi A. Review of vehicle engine efficiency and emissions. SAE Technical Paper 2017-01-0907. 2017, https://doi.org/10.4271/2017-01-0907.
[5] Zheng Y, Liu Y, Harold MP, Luss D. LNT–SCR dual-layer catalysts optimized for lean NO_x reduction by H_2 and CO. Appl Catal B Environ. 2014;148–149:311.
[6] Neely GD, Sarlashkar JV, Mehta D. Diesel cold-start emission control research for 2015-2025 LEV III emissions. SAE Int J Engines. 2013;6(2):1009–20.
[7] Roy S, Baiker A. NO_x storage–reduction catalysis: from mechanism and materials properties to storage–reduction performance. Chem Rev. 2009;109(9):4054.
[8] Epling WS, Campbell LE, Yezerets A, Currier NW, Parks JE. Overview of the fundamental reactions and degradation mechanisms of NO_x storage/reduction catalysts. Catal Rev. 2004;46(2):163.
[9] Lindholm A, Currier NW, Dawody J, Hidayat A, Li JH, Yezerets A, Olsson L. The influence of the preparation procedure on the storage and regeneration behavior of Pt and Ba based NO_x storage and reduction catalysts. Appl Catal B Environ. 2009;88(1):240.
[10] Mráček D, Kočí P, Marek M, Choi J-S, Pihl JA, Partridge WP. Dynamics of N_2 and N_2O peaks during and after the regeneration of lean NO_x trap. Appl Catal B Environ. 2015;166–167:509.
[11] Masdrag L, Courtois X, Can F, Duprez D. Effect of reducing agent (C_3H_6, CO, H_2) on the NO_x conversion and selectivity during representative lean/rich cycles over monometallic platinum-based NSR catalysts. Influence of the support formulation. Appl Catal B Environ. 2014;146:12.
[12] Ocampo F, Ohtake N, Southward BW. Recent developments for CeBa hybrid materials with enhanced properties for BS-6 NO_x storage applications. SAE Technical Paper 2017-26-123. 2017, https://doi.org/10.4271/2017-26-0123.
[13] Ji Y, Toops TJ, Crocker M. Effect of ceria on the storage and regeneration behavior of a model lean NO_x trap catalyst. Catal Lett. 2007;119(3):257.
[14] Ocampo F, Harle V, Ohtake N, Rohe R, Southward BW. Innovative hybrid rare earth and barium materials with enhanced properties for NO_x storage applications. SAE Int J Engines. 2015;8(3):1136.
[15] He L, Sun DF, Wang TY, Xu YH, Li RX. Synthesis of nano--CeO_2 hollow spheres with high adsorption activity via template-free solvothermal method. Chin J Rare Met. 2016;40(5):429.
[16] Jin H, Wang YY, Wang YT, Yang HB. Synthesis and properties of electrodeposited Ni–CeO_2 nano-composite coatings. Rare Met. 2018;37(2):148.
[17] Yang Q, Hu H, Wang SS. Preparation and desulfurization activity of nano-CeO_2/γ-Al_2O_3 catalysts. Rare Met. 2018;37(7):554.
[18] DiGiulio CD, Pihl JA, Choi J-S, Parks JE, Lance MJ, Toops TJ, Amiridis MD. NH_3 formation over a lean NO_x trap (LNT) system: effects of lean/rich cycle timing and temperature. Appl Catal B Environ. 2014;147:698.
[19] Auvray X, Pingel T, Olsson E, Olsson L. The effect gas composition during thermal aging on the dispersion and NO oxidation activity over Pt/Al_2O_3 catalysts. Appl Catal B Environ. 2013;129:517.
[20] Yang M, Li YP, Wang J, Shen MQ. Effects of CO_2 and steam on Ba/Ce-based NO_x storage reduction catalysts during lean aging. J Catal. 2010;271(2):228.
[21] Le Phuc N, Courtois X, Can F, Royer S, Marecot P, Duprez D. NO_x removal efficiency and ammonia selectivity during the NO_x storage-reduction process over Pt/BaO(Fe, Mn, Ce)/Al_2O_3 model catalysts. Part I: influence of Fe and Mn addition. Appl Catal B Environ. 2011;102(3):353.
[22] AL-Harbi M, Epling WS. Investigating the effect of NO versus NO_2 on the performance of a model NO_x storage/reduction catalyst. Catal Lett. 2009;130(1):121.
[23] Wang XY, Yu YB, He H. Effects of temperature and reductant type on the process of NO_x storage reduction over Pt/Ba/CeO_2 catalysts. Appl Catal B Environ. 2011;104(1–2):151.
[24] Clayton RD, Harold MP, Balakotaiah V, Wan CZ. Pt dispersion effects during NO_x storage and reduction on Pt/BaO/Al_2O_3 catalysts. Appl Catal B Environ. 2009;90(3):662.
[25] Dasari PR, Muncrief R, Harold M. Elucidating NH_3 formation during NO_x reduction by CO on Pt–BaO/Al_2O_3 in excess water. Catal Today. 2012;184(1):43.
[26] Wang J, Wang XT, Zhu JX, Wang JQ, Shen MQ. Elucidating N_2O formation during the cyclic NO_x storage and reduction process using CO as a reductant. Environ Sci Technol. 2015;49(13):7965.
[27] Zhu JX, Wang J, Wang JQ, Lv LF, Wang XT, Shen MQ. New Insights into the N_2O formation mechanism over Pt-BaO/Al_2O_3 model catalysts using H_2 as a reductant. Environ Sci Technol. 2015;49(1):504.
[28] Bártová Š, Kočí P, Mráček D, Marek M, Pihl JA, Choi J-S, Toops TJ, Partridge WP. New insights on N_2O formation pathways during lean/rich cycling of a commercial lean NO_x trap catalyst. Catal Today. 2014;231:145.
[29] Chatterjee D, Kočí P, Schmeißer V, Marek M, Weibel M, Krutzsch B. Modelling of a combined NO_x storage and NH_3-SCR catalytic system for diesel exhaust gas aftertreatment. Catal Today. 2010;151(3):395.
[30] Easterling V, Ji YY, Crocker M, Dearth M, McCabe RW. Application of spaciMS to the study of ammonia formation in lean NO_x trap catalysts. Appl Catal B Environ. 2012;123–124:339.